Applied Catalysis B: Environmental 181 (2016) 542–549

Contents lists available at ScienceDirect

Applied Catalysis B: Environmental

journal homepage: www.elsevier.com/locate/apcatb

Influence of the support material and the resulting particle distribution on the deposition of Ag nanoparticles for the electrocatalytic activity of benzyl bromide reduction

Bart Vanrenterghem[a], Bart Geboes[a,b], Sara Bals[c], Jon Ustarroz[b], Annick Hubin[b], Tom Breugelmans[a,b,*]

[a] University of Antwerp, Research Group Advanced Reactor Technology, Salesianenlaan 90, 2660 Hoboken, Belgium
[b] Vrije Universiteit Brussel, Research Group Electrochemical and Surface Engineering, Pleinlaan 2, 1050 Brussels, Belgium
[c] University of Antwerp, Research Group Electron Microscopy for Material Science, Groenenborgerlaan 171, 2020 Antwerpen, Belgium

ARTICLE INFO

Article history:
Received 1 June 2015
Received in revised form 6 August 2015
Accepted 12 August 2015
Available online 18 August 2015

Keywords:
Electrocatalysis
Cyclic voltammetry
Silver nanoparticles
Support material
Benzyl bromide

ABSTRACT

Silver nanoparticles (NPs) were deposited on nickel, titanium and gold substrates using a potentiostatic double-pulse method. The influence of the support material on both the morphology and the electrocatalytic activity of Ag NPs for the reduction reaction of benzyl bromide was investigated and compared with previous research regarding silver NPs on glassy carbon. Scanning electron microscopy (SEM) data indicated that spherical monodispersed NPs were obtained on Ni, Au and GC substrate with an average particle size of respectively 216 nm, 413 nm and 116 nm. On a Ti substrate dendritic NPs were obtained with a larger average particle density of 480 nm. The influence of the support material on the electrocatalytic activity was tested by means of cyclic voltammetry (CV) for the reduction reaction of benzylbromide (1 mM) in acetonitrile + 0.1 M tetrabutylammonium perchlorate (Bu_4NClO_4). When the nucleation potential (E_n) was applied at high cathodic overpotential, a positive shift of the reduction potential was obtained. The nucleation (t_n) and growth time (t_g) mostly had an influence on the current density whereas longer deposition times lead to larger current densities. For these three parameters an optimum was present. The best electrocatalytic activity was obtained with Ag NPs deposited on Ni were a shift of the reduction peak potential of 145 mV for the reaction of benzyl bromide was measured in comparance to bulk silver. The deposition on Au substrate yielded a positive shift of 114 mV. There was no indication of an altered reaction mechanism as the reaction was characterized as diffusion controlled and the transfer coefficients were in accordance with bulk silver. There was a beneficial catalitic activity measured due to the interplay between support and NPs. This resulted in a shift of the reduction peak potential of 34 mV (Ag NPs on Au) and 65 mV (Ag NPs on Ni) compared to Ag NPs on a GC substrate.

1. Introduction

In recent years nanomaterials of noble metals have received much attention because of their increased catalytic activity and applications in microelectronics [1–4]. Synthesis of metal nanoparticles (NPs) with a desired size and shape is becoming increasingly important due to the changes in physical and chemical characteristics [5–7] including bond distance, melting point, chemical reactivity, optical and electronic properties that differ from bulk materials. Depending on the application, NPs can be selected to achieve a particular purpose, of which the beneficial properties are caused by both the element materials and its morphology [1]. Due to the modified characteristics NPs can be used in electrocatalysis, where they can alter the catalytic properties.

There is a substantial interest in the electrochemistry and electrocatalysis of organic halides (RX) [8,9], due to the degradation of environmental pollution [10], investigation of the dissociative electron transfer mechanism [11] and the activation of the R—X bond [12]. The direct electrochemical reduction of RX in aprotic media on non-catalytic materials, proceeds at very negative electrode potentials [13]. Despite the intensive research, only a small number of metal electrodes, including Ag, Pd, Au and Cu, are known to possess a catalytic activity for the reduction reaction of RX [14]. NPs can provide a possible solution since they exhibit altered catalytic properties than the corresponding bulk material. Among the

* Corresponding author at: University of Antwerp, Research Group Advanced Reactor Technology, Salesianenlaan 90, 2660 Hoboken, Belgium.
E-mail address: tom.breugelmans@uantwerpen.be (T. Breugelmans).

http://dx.doi.org/10.1016/j.apcatb.2015.08.026
0926-3373/

known NPs such as Pt and Pd [15,16] literature mainly focusses on Ag NPs [7,17–19], due to the optical, spectroscopic and catalytic properties. Regardless the strong interest in Ag NPs, literature only reports a few examples where Ag NPs are electrodeposited for the RX activation [19,20].

A key aspect, which is often underestimated and to the best of our knowledge not studied yet for the halide reduction, is the influence of the support material on the electrocatalytic activity of NPs as electrocatalysts. Research of Hayden et all. [21] has already indicated the higher catalytic activity of titanium supported Au NPs than carbon supported ones for the CO oxidation. On the other hand, the catalytic activity of Pt NPs on a carbon supported surface is higher than titanium supported for the oxygen reduction reaction. It is clear that the NPs support plays a number of roles [2]. From a practical point of view, the support material acts as conductive bridge, connecting the NPs with an external circuit. Secondly the support provides a homogeneous distribution, with limited agglomeration and still obtains a high surface to volume ratio of the NPs. By introducing morphological defects the NPs catalyst can act as trapping sites for anchoring with the substrate. In addition the amendment of the NPs electronic properties due to the interaction with the support material can enhance the electrocatalytic activity [22]. Despite the fact that the occurrence of an improved catalytic activity by changing the support is well-known, the interaction and interplay between support material and catalytic activity of the NPs is significantly less understood. Changing the support has some practical applications regarding high activity, catalyst stability and formation of porous catalysts. For instance with the implementation of Ni or Ti in a microreactor the morphology of the supporting material can be easily controlled resulting in a longer life time cycle. In addition, a variation of the supporting material can reduce the high capital cost witch is nowadays the major disadvantage in fuel cell research [23].

The most common support materials for general electrodeposition of NPs are titanium [22], various types of carbon [24] or gold [25]. The current studies for the halide reduction by Ag NPs however are limited to glassy carbon (GC) [26–28]. In this paper new support materials for the electrodeposition of Ag NPs will be investigated for their influence on the catalytic activity of the RX bond activation. Ni, Ti, and Au are chosen as support materials. Ni and Ti are in general, like GC, considered as an inert material towards the halide reduction [14]. Moreover, both metals are less expensive than GC and possess a similar electrical resistivity. In addition, Au is investigated because, unlike the other support materials, it has a catalytic activity for the RX reduction. Furthermore, Au is often used in fundamental studies as it provides a stable surface to measure the influence on the catalytic activity and can be cleaned and characterized easily.

The aim of this study will be to compare the catalytic activity of bulk Ag and Ag NPs on a GC substrate with Ag NPs on Ni, Au and Ti for the reduction reaction of benzyl bromide which is often considered as a model molecule to study the halide reduction [13,14,29]. In this work the Ag NPs are electrochemically deposited on the different substrates with a high amount of control on their size and distribution using a double-pulse potentiostatic procedure. The NPs are fully characterized by scanning electron microscopy (SEM) while the electrochemical reactivity is tested by means of cyclic voltammetry.

2. Experimental

2.1. Deposition

The Ag NPs were deposited on planar electrode materials. The polishing procedure for Ni, Au and Ti consisted out of a sequential polishing with 1 μm and 0,3 μm alumina powder (Struers). A planar silver electrode was used as a benchmark and polished identical as the Au, Ni and Ti electrodes. After polishing, the electrodes were rinsed with ultra-pure water (18.2 MΩcm) and acetonitrile (BioSolve, HPLC grade) under sonication. The electrodeposition was carried out in a three electrode cell with a planar working electrode, a platinum wire as a counter electrode and an Ag/AgCl reference electrode. The reference electrode was separated from the working electrode through a salt bridge, preventing chloride or water contamination in the measurement medium. Unless stated otherwise, all mentioned potentials are reported vs. Ag/AgCl reference electrode. The electrodeposition was performed under potential control using a Biologic VSP-300. The electrolyte solution consisted of 0.1 M lithium perchlorate ($LiClO_4$) (Acros, 99<) and silver ions in the form of silver nitrate (1 mM) ($AgNO_3$) (99.9%, Sigma–Aldrich) in acetonitrile. Before each deposition measurement a precondition step with a high positive potential was applied to avoid spontaneous deposition on the support materials.

2.2. Morphological characterization

The surface morphology of the electrodeposited Ag NPs was studied using a FEI Quanta field emission gun 250 scanning electron microscope (SEM). Before each SEM measurement the electrodes were freshly rinsed and dried to air overnight. All measurements were conducted at an acceleration voltage of 20keV. IMAGEJ SXM 192.1 was used to extract the average particle diameter and density from thresholded SEM images.

2.3. Electrochemical characterization

The electrocatalytic activity of the nanostructured surfaces for the halide reduction of benzyl bromide was tested using cyclic voltammetry (CV). A conventional three electrode electrochemical cell was used with the nanostructured electrodes as working electrode. The reference and counter electrode were the same as used during the deposition measurements. The electrolyte solution contained 0.1 M tetrabutylammonium perchlorate (Bu_4NClO_4) (Acros, 99%+) in acetonitrile with benzyl bromide (1 mM) (Sigma–Aldrich, 98%).

3. Results and discussion

3.1. Deposition of NPs

To obtain size and shape controlled Ag NPs a potentiostatic double-pulse technique is used. In this procedure the morphology of the NPs can be easily controlled as the deposition is divided in two phases with a short nucleation pulse at more negative potential that is followed by a much longer growth pulse at a less negative potential. When the deposition proceeds under ideal circumstances nucleation occurs only within the first pulse and exclusive particle growth in the second pulse. During the deposition four parameters can be varied to control NPs morphology: nucleation potential (E_n), nucleation time (t_n), growth potential (E_g) and growth time (t_g). The dual pulse procedure is already intensively investigated [3,4,17,18,30], and described in detail allowing an easy set-up of the deposition variables on different support materials. In Table 1 the variation of the deposition parameters is tabulated in order to obtain NPs with a different size and particle distribution. These parameters are selected based on the investigation of the deposition potential of $AgNO_3$ on Ni, Au and Ti substrates and previous research regarding the deposition of Ag NPs on a GC electrode [31]. From the remaining of this work the electrodes are referred to

Table 1
Voltammetric parameters for the electrodeposition of AgNO3 (1 mM) in ACN + LiClO4 (0.1 M).

N°	Ni				Au				Ti			
	E_n (v)	t_n(s)	E_g (V)	t_g (s)	E_n (v)	t_n(s)	E_g (V)	t_g (s)	E_n (v)	t_n(s)	E_g (V)	t_g (s)
1	−0.3	1	0.25	100	−0.3	2	0.25	100	−1	2	−0.35	100
2	−0.4	1	0.25	100	−0.4	2	0.25	100	−0.8	2	−0.35	100
3	−0.5	1	0.25	100	−0.5	2	0.25	100	−0.6	2	−0.35	100
4	−0.6	1	0.25	100	−0.6	2	0.25	100	−0.8	1	−0.35	100
5	−0.5	0.75	0.25	100	−0.5	1	0.25	100	−0.8	3	−0.35	100
6	−0.5	0.5	0.25	100	−0.5	0.5	0.2	100	−0.8	2	−0.4	100
7	−0.5	1	0.3	100	−0.5	2	0.3	100	−0.8	2	−0.3	100
8	−0.5	1	0.2	100	−0.5	2	0.25	100	−0.8	2	−0.35	20
9	−0.5	0.5	0.25	20	−0.5	2	0.25	20	−0.8	2	−0.35	180
10	−0.5	0.5	0.25	180	−0.5	2	0.25	180	/	/	/	/

with the name of the support material, preceded by the deposition number from the first column.

3.2. Morphological characterization of Ag NPs

3.2.1. Influence of the nucleation phase on the morphology

At first the influence of E_n on the same support material is considered. In Fig. 1 SEM images of depositions with an E_n of −0.3 V, −0.4 V and −0.5 V on a Ni substrate are shown while the other deposition parameters are kept constant. Results indicate that a more negative E_n of −0.5 V (3Ni) leads to more nuclei, 8 particles/μm^2, compared to an E_n of −0.3 V (1Ni) where 5 particles/μm^2 are obtained. Although E_n at higher overpotential results in a larger particle density, it is remarkable to note that the particle size decreases. E_n of −0.3 V (a), −0.4 V (b) and −0.5 V (c) result in an average NPs size of 341 nm, 294 nm and 216 nm, respectively. With an E_n of −0.5 V a good dispersion of Ag NPs and limited presence of clusters and coagulations is obtained. Even though an increase is measured in the number of particles when E_n is further reduced until −0.6 V, there is a significant rise in present cluster. An optimum E_n to obtain monodisperse NPs is present at −0.5 V for the deposition on Ni while keeping the other deposition parameters constant.

Secondly the influence of E_n on different substrates is examined. When comparing the results of Ag NPs on Ni, Au and Ti substrates mutually and with Ag NPs on a GC substrate [31], it is clear that different types of Ag NPs are obtained. The effect of E_n on an Au surface is similar as with Ni, leading to spherical Ag NPs. Applying a high negative overpotential in the nucleation phase leads to a larger particle density. The optimum in E_n is present due to the formation of clusters when E_n is set more negative. A good particle distribution without coagulation is obtained when E_n is set on −0.5 V. Nucleation of Ag NPs on a Ti surface proceeds at a more negative potential. Unlike the deposition on Ni or Au, where spherical Ag NPs are being formed, deposition on Ti is leading to dendritic Ag NPs. With an E_n of −0.8 V NPs shapes are obtained with a sufficient coverage of the surface.

In Fig. 2 SEM images are shown of Ag NPs on 3Ni (a), 3Au (b) and 2Ti (c). The depositions on Au, Ni and GC substrates gives spherical particles NPs. The average particle size is smallest on GC with a particle size of 116 nm (not shown [31]). Particles on Ni and Au are larger with dimension of 216 nm and 413 nm respectively. In addition, the particle density is different, whereby GC has a particle density of 31 particles/μm^2 compared to 18 particles/μm^2 and 8 particles/μm^2 for Au and Ni. In contrast to these support materials deposition on Ti leads to larger dendritic Ag NPs with an average dimension of 480 nm. The NPs coverage on Ti was 43 particles/μm^2. Formation of dendritic NPs on Ti occurs through several stages and can be due to the higher overpotential or favourable surface tension of bulk Ti [32]. In addition the rate of growth of the dendrites is controlled by the kinetics of Ag ions in the solution which are opportune on Ti [33].

After studying E_n the influence of t_n is considered. To indicate the difference in t_n, SEM images are shown on a Ni surface at higher magnification (150.000×) in Fig. 3. Results show that with a longer t_n of 1 s (3Ni) (a) more NPs are deposited compared to 0.5s (6Ni) (b). Although t_n is longer, this does not result in larger particles. Moreover, with a shorter t_n larger and more isolated particles are obtained. Nucleation of 1s leads consistently to NPs with an average size of 216 nm while nucleation of 0.5s gives an average particle size of 327 nm. In addition, the particle density with a longer t_n in 3Ni (1s) is higher, 8 particles/μm^2 compared to 6Ni (0.5s), where the particles density is 4 particles/μm^2. As with E_n, t_n shows an optimum. If t_n is set longer than 1s this results in agglomeration of the particles.

When the influence of t_n on Au and Ti substrates is investigated similar results are obtained. On an Au substrate t_n can be set for 2s without the occurrence of agglomeration. However, with a longer t_n of 3s coagulation is still inevitable. Longer t_n did not influence the particle size but did increase the particle density. With a t_n of 1s (5Au) a particle density of 12 particles/μm^2 is found opposed to 18 particles/μm^2 with a t_n of 2s (3Au). Compared to Ni the same t_n (1s) results in Ag NPs of the same size (±220 nm) but with Au t_n can be set longer without the formation of clusters. When t_n is varied on Ti this results in more and larger dendritic NPs. For t_n longer than 2s (5Ti), a strong coagulation of NPs is visible. Shorter t_n of 1s (4Ti) on the other hand, results in more isolated NPs.

3.2.2. Influence of the growth phase on the morphology

The influence of E_g in the second stage of the deposition is minimal for Ni, Au and Ti. As long as the potential is set in the kinetic-controlled region where growth occurs, NPs of the same size are obtained without the formation of clusters.

t_g on the other hand, has a considerable impact on the particle size. Results for a Ni substrate show that a t_g of 20s (9Ni) leads to smaller NPs with an average size of 97 nm compared to 216 nm for a t_g of 100s (3Ni). Despite the fact that the NPs are smaller and still spherical in shape, the surface coverage is low (<1%) and there are more isolated particles present. On the contrary, when the growth time is extended to 180s strong agglomeration starts to occur, decreasing the favorable characteristics of the NPs. The influence of t_g is identical on an Au and Ti substrate than with a Ni substrate. A shorter t_g of 20s on 9Au leads to particles with an average size of 143 nm. Just as with Ni the surface coverage is low and there are many isolated particles present. On Ti a shorter t_g (8Ti) still leads to the formation of clusters and just as with Ni and Au a low surface coverage. Longer t_g (10Au and 9Ti) gives as well rise to the occurrence of agglomeration.

With deposition on 3Ni, 3Au and 2Ti Ag NPs are obtained with a good dispersion, without coagulation or, apart from Ti, the formation of clusters. In a next step the good morphological characteristics of the Ag NPs are checked to evaluated their electrocatalytic activity.

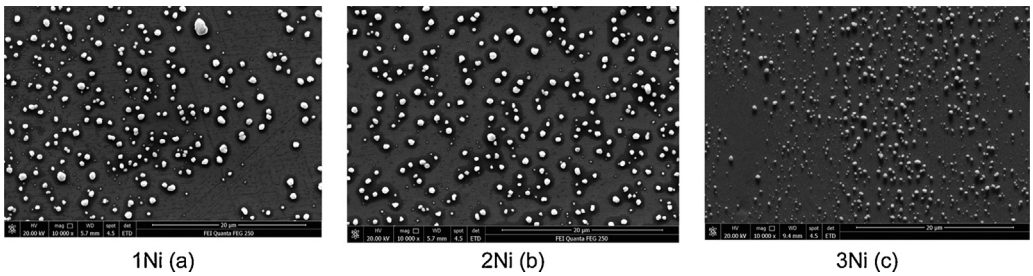

Fig. 1. SEM images (magnification 10000×) of Ag NPs on a Ni substrate deposited with nucleation potentials −0.3 V (a), −0.4 V (b) and −0.5 V (c) while the other deposition parameters are kept constant at t_n = 1 s, E_g = 0.25 V and t_g=100 s.

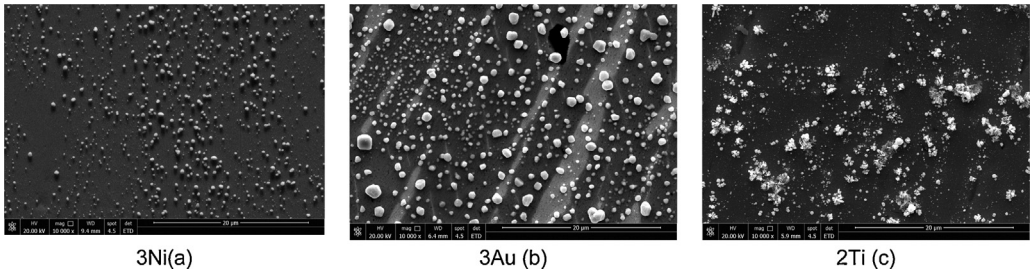

Fig. 2. SEM images (magnification 10000×) of Ag NPs on a Ni (a), Au (b) and Ti (C) deposited with E_n −0.5 V (Ni), −0.5 V (Au) and −0.8 V (Ti) while t_n = 1 s (Ni), t_n = 2 s (Au and Ti), E_g = 0.25 V (Ni and Au), E_g = −0.35 V (Ti), t_g = 100 s (Ni, Au and Ti) are kept constant.

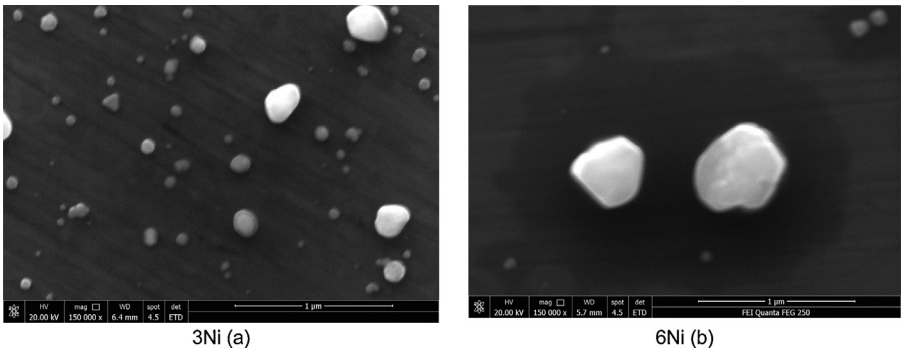

Fig. 3. SEM images (Magnification 150000×) of Ag NPs on Ni with a t_n of 1 s (a) and 0.5 s (b) with E_n = −0.5 V, E_g = 0.25 V and t_g = 100 s constant.

3.3. *Electrocatalytic activity of Ag NPs towards the halide reduction*

3.3.1. *Influence of nucleation phase on the catalytic activity*

At first, the influence of E_n is examined on the same support material. In Fig. 4 and Table 2 the influence of E_n on the electrocatalytic activity of Ag NPs on Ni is shown. Since a single reduction wave for the reduction reaction of benzyl bromide is present, this indicates an irreversible reaction mechanism. When E_n is shifted from −0.3 V (1Ni) until −0.5 V (3Ni) with identical t_n and growth parameters an increase in the reduction peak potential of 121 mV (Table 2) for the benzyl bromide reduction reaction is measured. With an E_n of −0.6 V (4Ni) the opposite effect is visible whereas the reduction peak potential decreases with 34 mV. This is expected, as formation of clusters and agglomeration of NPs at E_n of −0.6 V starts to occur. The catalytic activity can be related to particle shape. The peak current density is derived out of SEM measurements where the surface area is calculated out of the assumption that the NPs are hemispheric in shape. This calculation leads to a rough approximation of the surface area but gives a good impression of the current densities [33] as the determination of the EASA by Cu or Pb UPD for NPs still remains difficult. Although the surface area of 1Ni (0.081 cm^2), 2Ni (0.079 cm^2) and 3Ni (0.078 cm^2) is almost iden-

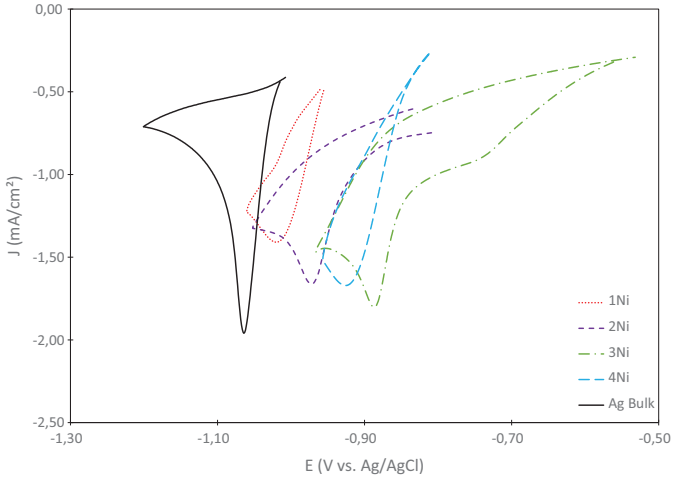

Fig. 4. CV features at 50 mV/s for the influence of E_n on the catalytic activity of Ag NPs on a Ni surface for the reduction reaction of benzyl bromide (1 mM). 1Ni = −0.3 V, 2Ni = −0.4 V, 3Ni = −0.5 V, 4Ni = 0.6 V, t_n = 1 s, E_g = 0.25 V, t_g = 100 s.

Table 2
Voltammetric data for benzyl bromide (1 mM) reduction in acetonitrile + 0.1 M Bu4NClO4 measured at 50 mVs^{-1} (E_p and J_p) with a variation of the deposition parameters on Ni.

	E_p(V)	J_p(mA/cm^2)	$I_p$vs. $v^{0.5}$	$I_p$vs. V	α[a]	α[b]
1Ni	−1.02	0.40	0.9908	0.9724	0.34	0.42
2Ni	−0.97	0.49	0.9924	0.9842	0.37	0.34
3Ni	−0.89	0.56	0.9975	0.9887	0.29	0.33
4NI	−0.92	0.44	0.9835	0.9653	0.28	0.31
5Ni	−0.89	0.45	0.9987	0.9641	0.31	0.29
6NI	−0.89	0.32	0.9982	0.9628	0.34	0.28
7Ni	−0.90	0.54	0.9894	0.9594	0.32	0.37
8Ni	−0.89	0.55	0.9705	0.9458	0.35	0.35
9Ni	−0.91	0.46	0.9978	0.9662	0.28	0.34
10Ni	−1.05	0.53	0.9934	0.9872	0.30	0.37
Bulk Ag	-1.04	1.26	0.9920	0.9663	0.29	0.36

[a] $\partial E_p/\partial \log v = -1.15RT/F\alpha$.
[b] $E_{p/2} - E_p = 1.857RT/F\alpha$.

tical, there is an increase of the current density visible when E_n is shifted towards more negative values of −0.5 V. A more homogeneous particle distribution can be the cause of this increase. At a more negative E_n of −0.6 V the opposite effect is visible whereas the peak current density decreases. As previous SEM results indicated (3.2.1.) this can be the result of the coagulation of NPs. When the current efficiency of the deposition process is considered and the currents are normalized per mg Ag, similar results are obtained for 1Ni (0.077 mA/mg Ag) 2Ni (0.074 mA/mg Ag) 3Ni (0.078 mA/ mg Ag) and 4Ni (0.076 mA/ mg Ag). In addition each deposition shows a good correlation of the current density and concentration of benzyl bromide (1, 2, 3 and 5 mM).

When Ag NPs on Ni are compared to bulk silver, all depositions show a positive shift towards the reduction potential of benzyl bromide. At an optimal E_n (−0.5 V) a shift of 145 mV is measured. The possibility that the reduction peak potential is derived from bulk Ni can be ruled out as research indicates that on bulk Ni the reduction peak is visible at −1.71 V [14,29]. To ensure that the shift of the reduction potential is due to Ag NPs and not to the occurrence of an alternative reaction, two indicators have been used. At first the scan rate of the reduction wave for benzyl bromide is varied from 50 mV/s until 500 mV/s. When plotting the peak current and the square root of the scan rate a better correlation is consistently found than with the current versus the scan rate (Table 2) so the reaction can be characterized as a diffusion controlled process.

Secondly the values of the electron transfer (ET) coefficient (α) are calculated from both the slope and the peak width (Table 2). Assuming a catalytic material, the ET can be considered as an inner sphere process, where the reaction proceeds in a concerted way on the surface and the value for α is expected to be less than 0.5. For the reduction reaction of benzyl bromide on bulk Ag literature reports values of 0.30 [34], [35]. With all the depositions (Table 2) the values of α are in compliance with bulk silver indicating that the reaction proceeds through the same one-electron concerted reaction mechanism.

$$RX + e^- \rightleftharpoons R^* + X^-$$
$$R^* + e^- \rightleftharpoons R^-$$

The variation of E_n on Au and Ti substrates has the same tendency on the catalytic activity as with Ni. The voltammetric data on Au and Ti is shown in Table 3. When E_n is varied on Au from −0.3 V (1Au) to −0.5 V (3Au) a shift of the reduction potential of 110 mV is obtained. The variation of E_n with Ti results in a shift of 76 mV (Table 3) between E_n of −0.6 V (3Ti) and −0.8 V (2Ti). E_n shows for both metals an optimum when the imposed potential is set more negative (−0.6 V for Au and −1 V for Ti) under the same conditions for t_n and growth phase. The calculated α (Table 3) indicate that the shift of the reduction peak potential is due to the NPs and not to an alternative reaction mechanism since for each deposition values of approximately 0,30 are obtained. Furthermore a better correlation is consistently found (Table 3) between the peak current and the square root of the scan rate than the peak current versus the scan rate whereby the reaction can be characterized as a diffusion controlled process. The obtained current efficiency on Ti is consequently low, 0.009 mA/ mg Ag.

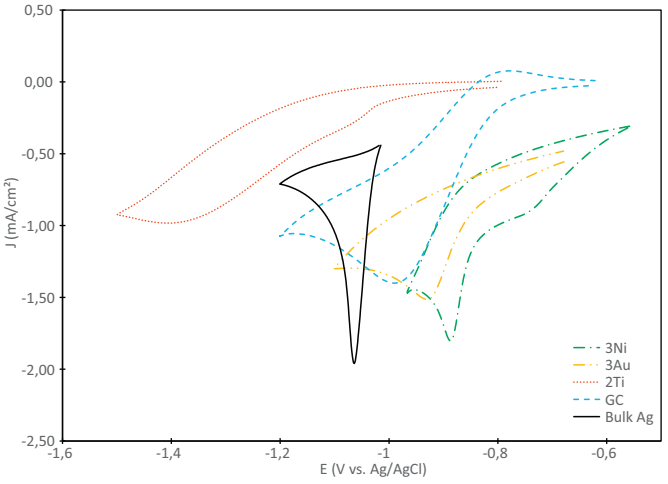

Fig. 5. Dependence of the catalytic activity on different support materials. CV features recorded at 50 mV/s in CH_3CN + 0.1 M Bu_4NClO_4 and benzyl bromide (1 mM).

In Fig. 5 and Table 4 the depositions with the largest shift in reduction peak potentials on the different support materials are presented. For each support material an irreversible peak is observed. All the curves of the reduction peaks have the typical features of an irreversible linear diffusion systems where the reduction occurs in a potential interval of −1.4 V until −0.8 V. Compared to bulk silver only Ti supported Ag NPs show a reduced activity whereby a reduction potential of −1.38 V is measured. The values of α (Table 4) however indicate that the decrease of the catalytic activity is not due to an alternative reaction mechanism but is indeed caused by the NPs and the interplay between NPs and the Ti support. This suggests that the electrocatalytic activity, for the reduction reaction of benzyl bromide, of Ag under the form of dendritic Ag NPs is decreased whereby the reduction potential is shape dependent. In addition to the fact that on Ti the morphology of the NPs is more difficult to control, no enhancement of the catalytic activity due to interaction between support and NPs is noticeable.

The Ag NPs deposited on Ni and Au do show to be more performing than Ag bulk (Table 4). The comparable α for the depositions and bulk Ag express the influence of NPs and not an alternative reaction mechanism. Spherical Ag NPs with an average size of 216 nm (Ni)

Table 3
Voltammetric data for the reduction reaction of benzyl bromide (1 mM) in acetonitrile + 0.1 M Bu4NClO4 measured at 50 mVs^{-1} (E_p and J_p) at Au and Ti.

	E_p (V)	J_p (mA/cm^2)	I_p vs. $v^{0.5}$	I_p vs. V	α^a	α^b
1Au	−1.04	0.39	0.9845	0.9494	0.31	0.34
2Au	−1.01	0..44	0.9821	0.9725	0.26	0.31
3Au	−0.93	0.52	0.9884	0.9625	0.26	0.32
4Au	−0.96	0.51	0.9723	0.9581	0.35	0.42
5Au	−0..94	0.45	0.9925	0.9857	0.32	0.37
6Au	−0.94	0.43	0.9942	0.9563	0.31	0.29
7Au	−0.93	0.52	0.9572	0.9508	0.29	0.35
8Au	−0,94	0.53	0.9886	0.9845	0.36	0.34
9Au	−0.93	0.48	0.9798	0.9590	0.27	0.32
10Au	−1.02	0.50	0.9957	0.9816	0.31	0.32
	E_p (V)	J_p (mA/cm^2)	I_p vs. $v^{0.5}$	I_p vs. V	α^a	α^b
1Ti	−1.42	0.17	0.9624	0.9440	0.36	0.37
2Ti	−1.38	0.19	0.9758	0.9562	0.30	0.39
3Ti	−1.45	0.19	0.9723	0.9691	0.33	0.31
4TI	−1.39	0.17	0.9661	0.9488	0.26	0.34
5Ti	−1.38	0.18	0.9842	0.9540	0.28	0.34
6TI	−1.4	0.18	0.9609	0.9504	0.33	0.38
7Ti	−1.39	0.18	0.9773	0.9709	0.31	0.39
8Ti	−1.39	0.16	0.9906	0.9813	0.32	0.40
9Ti	−1.38	0.17	0.9598	0.9389	0.35	0.38

Table 4
Voltammetric data for the reduction reaction of benzyl bromide (1 mM) in acetonitrile + 0.1 M Bu4NClO4 measured at 50 mVs^{-1} at different support materials.

	E_p (V)	J_p (mA/cm^2)	I_p vs. $v^{0.5}$	I_p vs. V	α^a	α^b
3Ni	−0.89	0.56	0.9975	0.9887	0.29	0.33
3Au	−0.93	0.52	0.9884	0.9625	0.26	0.32
2Ti	−1.38	0.19	0.9758	0.9562	0..3	0.39
Ag@GC	−0.98	0.71	0.9913	0.9732	0.26	0.36
Ag	−1.04	1.26	0.9805	0.9663	0.27	0..35

and 413 nm (Au) can enhance the catalytic activity. The current efficiency on Au (0.085 mA/cm^2) is comparable with Ni (0.078 mA/mg Ag). It can be noted that besides the improvement of catalytic activity by means of NPs, the support material also has an important influence. On GC, Ni and Au Ag NPs are present which provide an improvement of the activity but yet there is still a difference between them. The reduction potential for Ag NPs is −0.98 V (GC), −0.93 V (Au) and −0.89 V (Ni). The interplay between support material and NPs increases the catalytic activity. An explanation for the beneficial catalytic activity can be the assumption that one metal breaks the C—X bond and the other acts to reduce the absorbed intermediates [34]. These effect are most visible with Ag NPs on a Ni substrate.

After studying E_n, the influence of t_n is considered. Fig. 6 gives a representation of the influence of t_n on the catalytic activity of Ag NPs on a Ni substrate. In contrast to E_n, t_n has a very limited influence on the reduction peak potential. Adversely, the increase of the current density with a longer t_n is clearly visible. The higher current density of 3Ni compared to 6Ni (Table 2) can be, as previous SEM results indicated (Fig. 3), the result of a more homogeneous particle distribution.

The influence of t_n on Au (Table 3) is identical to Ni whereas the peak potential remains similar while the current density increases. It is interesting to notice that although t_n is the same for 3Ni and 5Au and the particle size is almost equal, there is a difference in the reduction peak potential. The effect of the Ag NPs is identical but due to the interaction with the support material a beneficial catalytic effect of 52 mV between 3Ni and 5Au is measured (Tables 2 and 3). For the deposition on Ti the apparent increase of current density is absent (Table 3). Although SEM images on Ti show an increase in coverage, the presence of cluster inhibits the increase of the current density.

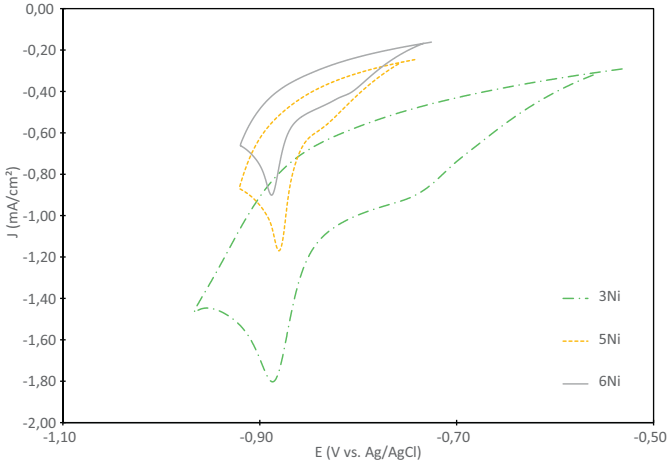

Fig. 6. CV features at 50 mV/s for the influence of t_n on the catalytic activity of Ag NPs on a Ni surface for the reduction reaction of benzyl bromide (1 mM). 3Ni = 1s, 5Ni = 0.75s, 6Ni = 0.5s, E_n = −0.5 V, E_g = 0.25 V, t_g = 100 s.

3.3.2. *Influence of the growth phase on the catalytic activity*

The variation of E_g in the growth phase appears to have a minimal effect on the catalytic activity for all the deposition on Ni, Au and Ti. When E_g is set on different values there is no shift or increase visible in both the reduction peak potential or current density (Tables 2 and 3). This is in accordance with the previous results of the SEM images whereby different E_g leads to NPs with similar size and shape.

t_g on the other hand has a clear influence on the catalytic activity. In Fig. 7 the influence of t_g on the same support material, Ni, is presented. When a longer t_g is applied in 3Ni (100s) compared to 9Ni

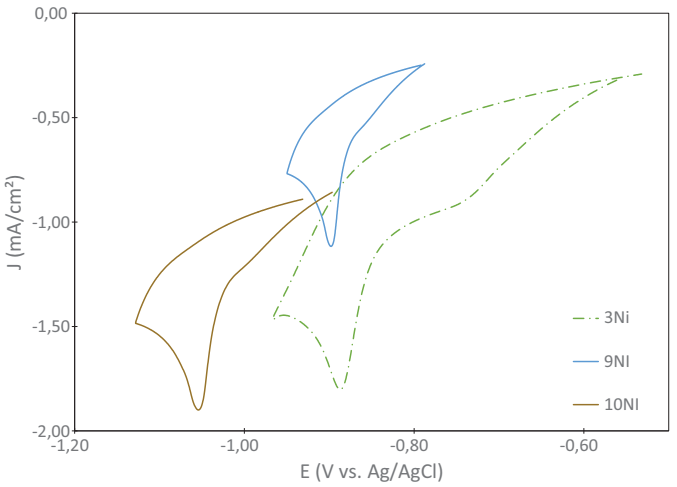

Fig. 7. CV features at 50 mV/s for the influence of t_g on the catalytic activity of Ag NPs on a Ni surface for the reduction reaction of benzyl bromide (1 mM). 3Ni = 100s, 9Ni = 20s, 10Ni = 180s, $E_n = -0.5$ V, $t_n = 1$ s $E_g = 0.25$ V.

(20s) a larger current density is measured. It is assumed that a more homogeneous particle distribution without coagulations increases the current density. The shift in reduction peak potential between 3Ni (100s) and 9Ni (20s) is limited. The smaller NPs in 9Ni (96 nm) obtained at a shorter t_g do not provide a further increase of the catalytic activity. On the contrary, larger NPs in 3Ni (216 nm) do appear to have a slightly beneficial catalytic effect of 12 mV. Nevertheless the difference remains small, making it difficult to discuss the influence of the particle size. When t_g is extended in 10Ni (180s) compared to 3Ni (100s) a drawback of 149 mV for the reduction peak potential is measured. These results are expected, as previous SEM results indicated that with a t_g of 180s agglomeration of NPs starts to occur. Cluster formation of the NPs decreases the catalytic activity and spherical NPs with a specific size boost the catalytic activity for the benzyl bromide reduction reaction. The smaller current density measured in 10Ni is explicable by the formation of clusters with a longer t_g.

The influence of t_g on the deposition of Ag NPs on Au is completely identical to Ni. Larger NPs in 10Au results in a decrease of the reduction peak potential and thus catalytic activity. In contrast with smaller NPs in 9Au, where the reduction potential remains constant (Table 3). On a Ti surface t_g had a minor influence on the catalytic activity. The difference in reduction potential is minimal with either a longer or shorter t_g. As mentioned, this can be caused by the presence of clusters or agglomeration of NPs.

4. Conclusion

Morphological controlled Ag NPs have been deposited on Ni, Au and Ti substrates by a potentiostatic double-pulse method in acetonitrile + 0.1 M $LiClO_4$ containing 1 mM $AgNO_3$. The morphology of the NPs is tuned by changing E_n, E_g, t_n and t_g. The variation of E_g did not influence the morphology or catalytic activity. The support material influences the size and shape of the NPs that are being formed during the electrodeposition. By changing E_n the size and the particle density of the NPs can be controlled. Although E_n at higher overpotential results in an increased catalytic activity, there is an optimum whereby more negative E_n leads to agglomeration of NPs. t_n and t_g have an influence on the size and coverage of NPs on the support. The duration of both parameters is limited due to the agglomeration of NPs. By controlling these parameters spherical Ag NPs can be obtained on Ni and Au and dendritic Ag NPs on Ti. Ag NPs on Ti did not show an improvement of the electrocatalytic activity compared to bulk Ag. With Ag NPs on GC, Au and Ni, however a positive shift of respectively 80 mV; 114 mV and 145 mV compared to bulk Ag is obtained. Since the reduction reaction of benzyl bromide is characterized as a diffusion controlled process and the calculated transfer coefficient α are approximately 0.3 there is no indication of an altered reaction mechanism. Independent of the NPs the interplay between support material and NPs plays an important role on the electrocatalytic activity. The suppression of adsorbed poisonous species and a change in the electronic band structure can enhance the catalytic activity. These effects are most visible with Ag NPs on a Ni substrate.

Acknowledgments

The Quanta 250 FEG microscope of the Electron Microscopy for Material Science group at the University of Antwerp was funded by the Hercules foundation of the Flemish Government. Sara Bals acknowledges financial support from European Research Council (ERC Starting Grant #335078-COLOURATOMS).

Appendix A. Supplementary data

Supplementary data associated with this article can be found, in the online version, at http://dx.doi.org/10.1016/j.apcatb.2015.08.026.

References

[1] H. Liu, F. Favier, K. Ng, M. Zach, R. Penner, Size-selective electrodeposition of meso-scale metal particles: a general method, Electrochim. Acta 47 (December (5)) (2001) 671–677.
[2] S.E.F. Kleijn, S.C.S. Lai, M.T.M. Koper, P.R. Unwin, Electrochemistry of nanoparticles, Angew. Chem. Int. Ed. Engl. 53 (April (14)) (2014) 3558–3586.
[3] M. Ueda, H. Dietz, A. Anders, H. Kneppe, A. Meixner, W. Plieth, Double-pulse technique as an electrochemical tool for controlling the preparation of metallic nanoparticles, Electrochim. Acta 48 (December (4)) (2002) 377–386.
[4] R.E. Dávila-Martínez, L.F. Cueto, E.M. Sánchez, Electrochemical deposition of silver nanoparticles on TiO2/FTO thin films, Surf. Sci. 600 (September (17)) (2006) 3427–3435.
[5] D.F. Sanchez, R. Moiraghi, F.P. Cometto, M.A. Pérez, P.F.P. Fichtner, P.L. Grande, Morphological and compositional characteristics of bimetallic core@shell nanoparticles revealed by MEIS, Appl. Surf. Sci. 330 (March) (2015) 164–171.
[6] A. Shukla, B. a Makwana, Facile synthesis of silver nanoparticle and their potential application, vol. 2, no. 4, pp. 84–92, 2014.
[7] A.A. Isse, S. Gottardello, C. Maccato, A. Gennaro, Silver nanoparticles deposited on glassy carbon. Electrocatalytic activity for reduction of benzyl chloride, Electrochem. commun. 8 (November (11)) (2006) 1707–1712.
[8] H.J. Schäfer, Contributions of organic electrosynthesis to green chemistry, Comptes Rendus Chim. 14 (July (7–8)) (2011) 745–765.
[9] E. Duñach, M.J. Medeirosb, S. Oliveroa, Intramolecular reductive cyclisations using electrochemistry: development of environmentally friendly synthetic methodologies, New J. Chem. 30 (11) (2006) 1534.
[10] C. Durante, A.A. Isse, G. Sandonà, A. Gennaro, Electrochemical hydrodehalogenation of polychloromethanes at silver and carbon electrodes, Appl. Catal. B Environ. 88 (May (3–4)) (2009) 479–489.
[11] A. a Isse, S. Gottardello, C. Durante, A. Gennaro, Dissociative electron transfer to organic chlorides: electrocatalysis at metal cathodes, Phys. Chem. Chem. Phys. 10 (May (10)) (2008) 2409–2416.
[12] V. Durante, L. Perazzolo, M. Perini, G. Granozzi, A. Gennaro, Electrochemical activation of carbon–halogen bonds: electrocatalysis at silver/copper nanoparticles, Appl. Catal. B Environ. 158–159 (October) (2014) 286–295.
[13] V. Jouikov, J. Simonet, The one-electron cleavage of benzylic bromides at palladium and palladized cathodes: benzyl radicals generation and immobilization onto solid interfaces, Electrochem. commun. 12 (March (3)) (2010) 331–334.
[14] C. Bellomunno, D. Bonanomi, L. Falciola, M. Longhi, P.R. Mussini, L.M. Doubova, G. Di Silvestro, Building up an electrocatalytic activity scale of cathode materials for organic halide reductions, Electrochim. Acta 50 (April (11)) (2005) 2331–2341.
[15] B. Geboes, I. Mintsouli, B. Wouters, J. Georgieva, A. Kakaroglou, S. Sotiropoulos, E. Valova, S. Armyanov, A. Hubin, T. Breugelmans, Surface and electrochemical characterisation of a Pt-Cu/C nano-structured electrocatalyst, prepared by galvanic displacement, Appl. Catal. B Environ. 150–151 (May) (2014) 249–256.
[16] N.V. Long, T.D. Hien, T. Asaka, M. Ohtaki, M. Nogami, Synthesis and characterization of Pt–Pd nanoparticles with core–shell morphology:

nucleation and overgrowth of the Pd shells on the as-prepared and defined Pt seeds, J. Alloys Compd. 509 (July (29)) (2011) 7702–7709.
[17] W. Plieth, H. Dietz, A. Anders, G. Sandmann, A. Meixner, M. Weber, H. Kneppe, Electrochemical preparation of silver and gold nanoparticles: characterization by confocal and surface enhanced Raman microscopy, Surf. Sci. 597 (December (1–3)) (2005) 119–126.
[18] G. Sandmann, H. Dietz, W. Plieth, Preparation of silver nanoparticles on ITO surfaces by a double-pulse method, J. Electroanal. Chem. 491 (September (1–2)) (2000) 78–86.
[19] C. An, Y. Kuang, C. Fu, F. Zeng, W. Wang, H. Zhou, Study on Ag–Pd bimetallic nanoparticles for electrocatalytic reduction of benzyl chloride, Electrochem. Commun. 13 (December (12)) (2011) 1413–1416.
[20] T. Maiyalagan, Synthesis, characterization and electrocatalytic activity of silver nanorods towards the reduction of benzyl chloride, Appl. Catal. A Gen. 340 (June (2)) (2008) 191–195.
[21] B.E. Hayden, D. Pletcher, J.-P. Suchsland, L.J. Williams, The influence of support and particle size on the platinum catalysed oxygen reduction reaction, Phys. Chem. Chem. Phys. 11 (October (40)) (2009) 9141–9148.
[22] B.E. Hayden, D. Pletcher, J.-P. Suchsland, Enhanced activity for electrocatalytic oxidation of carbon monoxide on titania-supported gold nanoparticles, Angew. Chem. Int. Ed. Engl. 46 (19) (2007) 3530–3532.
[23] C.-J. Zhong, J. Luo, B. Fang, B.N. Wanjala, P.N. Njoki, R. Loukrakpam, J. Yin, Nanostructured catalysts in fuel cells, Nanotechnology 21 (6) (2010) 062001.
[24] R.L. Mccreery, Advanced carbon electrode materials for molecular electrochemistry, Adv. Carbon Electrode Mater. Mol. Electrochem. 108 (June) (2008) 2646–2687.
[25] F.J. Vidal-Iglesias, J. Solla-Gullón, P. Rodrıíguez, E. Herrero, V. Montiel, J.M. Feliu, A. Aldaz, Shape-dependent electrocatalysis: ammonia oxidation on platinum nanoparticles with preferential (100) surfaces, Electrochem. Commun. 6 (October (10)) (2004) 1080–1084.
[26] A. a, S.G. Isse, C.M. ottardello, A.G. accato, Silver nanoparticles deposited on glassy carbon. Electrocatalytic activity for reduction of benzyl chloride, Electrochem. Commun. 8 (November (11)) (2006) 1707–1712.
[27] A. Gennaro, A.A. Isse, C.L. Bianchi, P.R. Mussini, M. Rossi, Is glassy carbon a really inert electrode material for the reduction of carbon–halogen bonds? Electrochem. Commun. 11 (October (10)) (2009) 1932–1935.
[28] L. Perini, C. Durante, M. Favaro, S. Agnoli, G. Granozzi, A. Gennaro, Electrocatalysis at palladium nanoparticles: effect of the support nitrogen doping on the catalytic activation of carbonhalogen bond, Appl. Catal. B Environ. 144 (January) (2014) 300–307.
[29] A. a, A.D. Isse, G. e, A.G. iusti, L.F. ennaro, P.R.M. alciola, Electrochemical reduction of benzyl halides at a silver electrode, Electrochim. Acta 51 (June (23)) (2006) 4956–4964.
[30] V. Bostanov, W. Obretenov, Shape and growth rate of monoatomic layers during the electrocrystallization of silver on a screw-disclocation free (111) crystal face, Electrochim. Acta 34 (August (8)) (1989) 1193–1196.
[31] B. Geboes, B. Vanrenterghem, J. Ustarroz, D. Pauwels, Influence of the morphology of electrodeposited nanoparticles on the activity of organic halide reduction, Chem. Eng. Trans. 41 (2014) 73–78.
[32] J. Zhu, A. Kamiya, T. Yamada, W. Shi, K. Naganuma, K. Mukai, Surface tension, wettability and reactivity of molten titanium in Ti/yttria-stabilized zirconia system, Mater. Sci. Eng. A 327 (2) (2002) 117–127.
[33] J.O'M. Bockris, J.L. Barton, The electrolytic growth of dendrites from ionic solutions, J. Electroanal. Chem. 268 (September (1335)) (1962), p. Proc. R. Soc.
[34] A.A. Isse, G. Berzi, L. Falciola, M. Rossi, P.R. Mussini, A. Gennaro, Electrocatalysis and electron transfer mechanisms in the reduction of organic halides at Ag, J. Appl. Electrochem. 39 (January (11)) (2009) 2217–2225.
[35] D.A. Cantane, F.E.R. Oliveira, S.F. Santos, F.H.B. Lima, Synthesis of Pt-based hollow nanoparticles using carbon-supported Co@Pt and Ni@Pt core–shell structures as templates: electrocatalytic activity for the oxygen reduction reaction, Appl. Catal. B Environ. 136–137 (June) (2013) 351–360.